

Efficient and reliable modeling of large π -electron systems with the Pariser–Parr–Pople Hamiltonian and pCCD-based methods

Zahra Karimi, Somayeh Ahmadkhani,^{*} Katharina Boguslawski, and Paweł Tecmer[†]

*Institute of Physics, Faculty of Physics, Astronomy,
and Informatics, Nicolaus Copernicus University in Toruń,
Toruń, Grudziądzka 5, 87-100 Toruń, Poland*

(Dated: August 27, 2025)

Model Hamiltonians offer a cost-effective way to capture the key physics of large π -conjugated systems. In this work, we combine the Pariser–Parr–Pople (PPP) model Hamiltonian with pair Coupled Cluster Doubles (pCCD)-based methods to study the ground- and excited-state electronic structures of polycyclic aromatic hydrocarbons (PAHs). The model Hamiltonian implementation is done in the open-source PyBEST software package, where numerous pCCD-type models are available. We investigate canonical Hartree–Fock and natural pCCD-optimized orbitals to compute ground- and excited-state properties using pCCD and its linear response extension. Their performance is compared with configuration-interaction-based methods. Finally, we introduce a generalized parameterization of the long-range Coulomb interaction using a rescaled interaction prefactor to adopt the PPP parameters to the pCCD approach and the localized nature of the pCCD orbitals. Our results demonstrate that pCCD-based methods, combined with a suitably parametrized PPP model, provide a reliable and scalable framework for studying the optoelectronic properties of large π -extended systems relevant to organic electronics.

Keywords: PPP Hamiltonian, coupled cluster (CC), pair Coupled Cluster Doubles (pCCD), orbital optimized CC, linear response CC, electronic excitations, electron correlation, transition dipole moments

I. INTRODUCTION

Reliable modeling of the electronic structures and properties of large π -electron systems, such as organic semiconductors and other conjugated molecules, remains a real challenge for present-day computational physics, chemistry, and materials science. [1–3] Such systems are usually large in size and exhibit a non-negligible amount of strong (static) electron correlation effects [4, 5] due to their near-degenerate π -electron networks, which limits the application of standard electronic structure

^{*} so.ahmadkhani@gmail.com

[†] ptecmer@fizyka.umk.pl

methods. [3, 6–10]

While *ab initio* quantum chemistry methods, such as the full configuration interaction (FCI), offer the most accurate description of electronic structures, [11, 12] their computational cost scales exponentially with system size, rendering them impractical for large molecules or extended systems. [13] To address this, various approximate approaches have been developed. For example, truncated configuration interaction (CI) methods, such as configuration interaction singles (CIS) and configuration interaction singles and doubles (CISD), and the multi-configurational self-consistent field (MC-SCF) methods, [14, 15] include key electronic configurations to improve accuracy while reducing cost. [16] These approaches can capture important features of excited states and potential energy surfaces but still suffer from rapid growth in the number of configurations with system size and from size-consistency problems when the orbitals are not optimized in the correlation treatment. An alternative to reduce computational cost is to use the density matrix renormalization group (DMRG) algorithm. [8, 17–27] On the other hand, single-reference quantum chemical methods, such as density functional theory (DFT) [28] or coupled-cluster (CC) theory [29–33] are typically computationally more attractive when modeling large-scale systems. However, they often struggle with quasi-degenerate states and cannot capture the essential physics of π -extended systems. [34, 35]

One strategy to address these challenges involves using simplified yet physically meaningful model Hamiltonians that reduce computational cost while retaining the essential physics of the system. The Hückel model [36, 37] provides a tight-binding description of π -electron systems based solely on one-electron terms. The Hubbard model, [38] introduced to describe electron interactions in narrow energy bands, extends this by including an on-site Coulomb repulsion term, thereby accounting for short-range electron correlation in a minimal way. The Pariser–Parr–Pople (PPP) model, developed by Pariser and Parr [39, 40] and Pople, [41] extends the Hückel model by explicitly incorporating electron-electron interactions via a semi-empirical parameterization. The theoretical foundation and improved parameterization for conjugated systems have been established over the years. [42–47] Adamowicz and co-workers [48] proposed a localized semi-empirical coupled cluster framework that utilizes ethylene-like π -molecular orbitals, enabling efficient computation of (hyper)polarizabilities in nonalternant hydrocarbons.

To further enhance the efficiency of electronic structure calculations with the PPP model, we can combine them with geminal-based methods. [49–55] One promising geminal model is the Antisymmetric Product of 1-reference Orbital Geminals (AP1roG), also known as pair Coupled Cluster Doubles (pCCD). [56–58] When combined with an efficient orbital optimization protocol [57–61]

and dynamic energy corrections, [62–66] pCCD-based approaches emerge as versatile and effective tools for modeling large-scale molecules, including organic building blocks and complexes containing transition metals, lanthanides, and actinides. [10, 66–78] Recent quantum chemical calculations on organic electronic molecules [9, 10, 77–79] show remarkably good predictive power at low computational cost to standard electronic structure methods. Yet, the orbital optimized pCCD-based methods improve upon the canonical Hartree–Fock orbitals in quasi-degenerate systems like long polymer chains or π -extended systems. [9, 77, 79] To that end, in this work, we implement the Tight-Binding/Hückel and PPP model Hamiltonians in the open-source PyBEST software package and use them with pCCD-based methods. The Python-based implementation has a modular design, which differs from existing programs. [80, 81] Our application focus is set on modeling electronic structures and UV-Vis spectra of selected excited-state polycyclic aromatic hydrocarbons (PAHs).

II. THEORY

A. Model Hamiltonians

The PPP Model Hamiltonian, commonly used to describe the electronic structure of conjugated π -electron systems, is given by

$$\hat{H}_{\text{PPP}} = \sum_{\langle i,j \rangle} t_{ij} \left(\hat{c}_i^\dagger \hat{c}_j + \hat{c}_j^\dagger \hat{c}_i \right) + \sum_{\langle i,j \rangle} V_{ij} n_i n_j + \sum_i U n_{i\uparrow} n_{i\downarrow}, \quad (1)$$

where the terms represent distinct physical interactions within the π -electron system. The first term in Eq. 1 describes the hopping of electrons between neighboring sites i and j , with t_{ij} being the hopping integral quantifying the probability amplitude for an electron to move between these sites. The operators \hat{c}_i^\dagger and \hat{c}_j are the creation and annihilation operators, respectively, for an electron at sites i and j . The summation $\langle i, j \rangle$ is restricted to neighboring pairs of sites. The second term in Eq. (1) accounts for the long-range Coulomb repulsion between electrons at sites i and j . The parameter V_{ij} represents the magnitude of this interaction and typically decreases with the distance between the sites. Here, $n_i = \hat{c}_i^\dagger \hat{c}_i$ is the particle number operator, denoting the number of electrons at site i . This term models the electron–electron repulsion between two π -orbitals located on sites i and j using a distance-dependent Coulomb integral. [82] In the case of $i = j$, this boils down to the on-site Coulomb interaction (term three in eq. (1)). The original expression for V_{ij} was proposed

by Ohno, [82]

$$V_{ij} = \frac{U}{\sqrt{1 + \left(\frac{R_{ij}}{r_0}\right)^2}}, \quad (2)$$

where U is the on-site Coulomb repulsion, R_{ij} is the distance between sites (atoms) i and j , and r_0 is an empirical screening length. The above formula satisfies the correct limiting behavior, namely, $V_{ii} = U$ for $R_{ij} = 0$ and $V_{ij} \sim 1/R_{ij}$ for large interatomic distances. Eq. (2) was derived under the *zero differential overlap* (ZDO) approximation, where all overlap integrals between different atomic orbitals are neglected,

$$S_{ab} = \int \chi_a(\mathbf{r})\chi_b(\mathbf{r}) d\mathbf{r} \approx 0 \quad \text{for } a \neq b, \quad (3)$$

which significantly simplifies the evaluation of molecular integrals and allows for analytical parametrizations like Eq. (2). A commonly used Ohno parametrization reads

$$V_{ij} = \frac{U}{\kappa_{ij} \sqrt{1 + 0.6117 R_{ij}^2}}, \quad (4)$$

where κ_{ij} encodes dielectric screening, incorporating effects such as electronic delocalization, polarization, and environmental screening. That specific parameterization has been successfully used in various electronic structure methods, including the multi-reference singles-doubles configuration interaction methodology (MRSDCI), [45, 83, 84] as well as traditional coupled cluster approaches. [85]

B. pCCD-based Methods

Coupled cluster theory [29–31] with single and double excitations (CCSD) is widely employed to describe dynamic (weak) electron correlation. [4, 33] However, it often fails in systems with strong (static, non-dynamic) electron correlation. [58, 69, 86] Such multi-reference problems can be modeled within a multi-reference formulation of CC theory. [87–90] A cheaper alternative is to address the limitations of single-reference CC theory is to simplify the CCSD ansatz even further. One such simplified variant is the pair-coupled cluster doubles (pCCD) method that restricts the cluster operator to electron-pair excitations only. [56] This restriction significantly reduces computational cost while enabling a reliable treatment of static electron correlation. [9, 58, 67, 68, 77, 78, 91]

The pCCD wave function is defined as

$$|\Psi_{\text{pCCD}}\rangle = e^{\hat{T}_{\text{p}}}|\Phi_0\rangle, \quad (5)$$

where $|\Phi_0\rangle$ is some reference Slater determinant and \hat{T}_p is the cluster operator that includes only seniority-zero double (that is, electron-pair) excitations,

$$\hat{T}_p = \sum_i^{\text{occ}} \sum_a^{\text{virt}} t_{i_\uparrow i_\downarrow}^{a_\uparrow a_\downarrow} \hat{c}_{a_\uparrow}^\dagger \hat{c}_{a_\downarrow}^\dagger \hat{c}_{i_\downarrow} \hat{c}_{i_\uparrow}. \quad (6)$$

In the above equation, the sums run over all occupied (virtual) orbitals of the reference determinant $|\Phi_0\rangle$. The corresponding pCCD energy is given by (for any Hamiltonian \hat{H})

$$E = \langle \Phi_0 | e^{-\hat{T}_p} \hat{H} e^{\hat{T}_p} | \Phi_0 \rangle \quad (7)$$

and the cluster amplitudes are determined from the amplitude equations by projecting against all pair-excited determinants $\langle \Phi_{i_\uparrow i_\downarrow}^{a_\uparrow a_\downarrow} | = \langle \Phi_0 | \hat{c}_{i_\uparrow}^\dagger \hat{c}_{i_\downarrow}^\dagger \hat{c}_{a_\downarrow} \hat{c}_{a_\uparrow}$,

$$\langle \Phi_{i_\uparrow i_\downarrow}^{a_\uparrow a_\downarrow} | e^{-\hat{T}_p} \hat{H} e^{\hat{T}_p} | \Phi_0 \rangle = 0. \quad (8)$$

pCCD is formally equivalent to a full configuration interaction (FCI) solution in the seniority-zero sector, provided the orbitals are optimized to define the pairing structure. [57–61] This orbital optimization, known as the orbital-optimized pCCD (oo-pCCD) variant, is crucial for maximizing the accuracy of the method when modeling strong correlation and retrieving size-consistency of potential energy surfaces. [58, 91]

Recent developments have significantly extended the applicability of pCCD-based methods to excited-state calculations. [92, 93] The linear-response formulation of pCCD (LR-pCCD) and its variants, such as LR-pCCD+S, enable efficient computations of singly and doubly excited state energies and transition properties within the pair-excitation manifold [94]. Equation-of-motion post-pCCD methods have also been developed to capture excited states beyond the seniority-zero space. [95] We should note the EOM and LR formalisms share the same excitation energies, but differ in the treatment of excited states dipole moments. [33]

Due to their favorable balance between accuracy and computational cost, pCCD-based methods are especially useful for modeling large π -conjugated systems relevant to organic electronics. [9, 10, 78, 79] They provide a scalable and reliable approach for studying the electronic properties of molecular building blocks of bulk heterojunction organic solar cells (OSCs), aiding in the rational design of efficient organic materials. Leveraging the synergistic potential of pCCD-based methods and model Hamiltonians promises to significantly advance the scalability and predictive power, unlocking new frontiers in the study of large-scale quantum systems.

C. Dipole Integrals in Physical Model Hamiltonians

In semi-empirical approaches, such as the PPP model with Ohno parametrization, the evaluation of dipole moments does not rely on atom-centered basis functions or explicit momentum integrals. Instead, dipole integrals are constructed directly from atomic coordinates, consistent with the tight-binding formalism.

To compute the dipole moment vector $\vec{\mu}$, we need to define effective momentum integrals in the x , y , and z directions as follows

$$(\mu_\alpha)_{ij} = S_{ij} \cdot \frac{1}{2}(r_i^\alpha + r_j^\alpha), \quad \alpha \in \{x, y, z\}, \quad (9)$$

where r_i^α is the α -component of the Cartesian coordinate of atom i , S_{ij} is an overlap-like matrix (defined below), and $|i\rangle$ denotes a localized orbital at site i . This formulation incorporates both the spatial extent of π -orbitals and their mutual overlap, leading to a more accurate representation of the off-diagonal dipole moment contributions.

To account for spatial proximity and nonorthogonality between orbitals, we also define an overlap-like matrix \mathbf{S} using a Gaussian decay function,

$$S_{ij} = \exp\left(-\left(\frac{|\vec{r}_i - \vec{r}_j|}{\lambda}\right)^2\right), \quad (10)$$

where λ is a tunable decay parameter controlling the effective range of orbital overlap.

The final ground state dipole moment is then computed using the electronic density matrix ρ as, [96]

$$D_\alpha = \text{Tr}[\mu_\alpha \cdot \rho], \quad \alpha \in \{x, y, z\}. \quad (11)$$

This approach ensures a physically meaningful estimate of the dipole moment within a minimal basis model without invoking ab initio basis functions or momentum integral evaluations in an atom-centered basis set. [97]

In typical conjugated systems (e.g., benzene or graphene fragments), the C–C bond length is nearly constant (≈ 1.40 – 1.42 Å), comprising the $2p_z$ orbitals with a fixed spatial extent. Thus, the overlap matrix (S_{ij}) between neighboring atoms will also be nearly uniform (e.g., 0.25–0.33) for nearest neighbors. [82] One can use various computational approaches, such as linear-response or equation-of-motion (EOM) based methods, to obtain excited-state dipole moments. Still, only the linear response formalism ensures that transition properties scale correctly with system size. To that end, we compute oscillator strengths using the linear-response method, [94] and pCCD response density matrices to investigate the intensity of electronic transitions. [96, 98]

III. RESULTS

A. Refinement of Model Hamiltonian Parameters

We implemented the PPP model Hamiltonian into the open-source PyBEST software package [99, 100] and used the conventional Ohno expression of eq. (2) and (4) for the electron–electron interaction. We tested two commonly used parameter sets: a screened case with $U = 8$ eV, $\kappa = 2$, and $t = 2.4$ and the standard parameters $U = 11.13$ eV, $\kappa = 1$, and $t = 2.4$ as widely adopted in the literature. [83, 101] While these parameters yield reasonable results at the HF level (the computed orbital/site energies reproduce other theoretical data from Ref. [83] and represent a good approximation to the experimental optical gap of investigated systems), pCCD-based methods are highly sensitive to the model parameters and fail to produce physically meaningful results for either set. Upon the pCCD orbital optimization, [58, 59, 61] the delocalized HF sites, mimicking the $2p_z$ orbitals of C, become localized (symmetry broken), which affects the resulting 1- and 2-electron integrals. To that end, the standard HF parameters in the PPP model require reoptimization.

To identify a consistent and physically motivated parameter set for the PPP Hamiltonian compatible with pCCD-based methods (for ground and excited states), we carried out a series of parameter scans guided by experimental excitation energies [102, 103] of the Benzo[a]coronene ($C_{28}H_{14}$) and Naphtho[8,1,2-abc]coronene ($C_{30}H_{14}$) shown in Figure 1.

To that end, we fine-tuned the PPP parameters for canonical HF orbitals and the pCCD-optimized ones. Specifically, we investigated whether a single set of model parameters could accurately describe the electronic structure of multiple PAHs as displayed in Figure 1 within the pCCD framework. We optimized the PPP Hamiltonian by scanning a series of parameters guided by experimental excitation energies. For each molecular structure (e.g., $C_{28}H_{14}$ and $C_{30}H_{14}$), we generated contour plots in which the x-axis represents the on-site interaction strength U , the y-axis corresponds to the hopping integral t , and the contour levels indicate the computed excitation energies (cf. Figure 4). These plots were generated for several fixed values of the dielectric screening parameter k , which appears in the Ohno-like expression for long-range electron–electron interactions [80, 82].

We observed that no unique combination of U , t , and κ parameter set could simultaneously reproduce the excitation energies of both benchmarked molecules. In particular, different optimal values of κ were required to match experimental data for each molecule. Since k should remain constant across all systems under study, this highlights the limitation of the standard PPP model,

which lacks sufficient flexibility to describe electronic properties across multiple PAHs as reliably as possible using a common screening parameter. To overcome this limitation, we introduced a global scaling factor $U' = \frac{U}{\kappa}$ that rescales the entire electron–electron interaction matrix while preserving its distance dependence (*vide infra* and *cf.* eq. (12)). Based on experimental fitting, the long-range Coulomb interaction V_{ij} is often parameterized using the Ohno formula of eq. (4). According to this parameterization, r_0 is typically taken as $r_0 \approx 1.28$, in the same unit as R_{ij} . Since each computational method requires a distinct set of experimentally fitted parameters for the Ohno formula, we adopt a smaller value of $r_0 = 0.25$, as mentioned in Ref. 82, which is motivated by the typical magnitude of overlap integrals between neighboring $2p_\pi$ orbitals in conjugated systems, which is usually in the range of 0.25 to 0.33. [82] This choice corresponds to stronger short-range interactions and leads to a faster decay of the Coulomb potential with distance, as shown in Figure 2. It also reflects a more localized interaction picture consistent with the minimal-overlap assumption often used in semi-empirical models such as PPP. The modified Ohno equations then reads

$$V_{ij} = \frac{U'}{\sqrt{1 + (R_{ij}/0.25)^2}}. \quad (12)$$

1. First Vertical Excitation Energy Maps and Parameter Sensitivity for the Canonical Case

To investigate the impact of model parameterization on excitation energies, we generated contour plots of the first excited state as functions of the hopping integral t and the screened Coulomb interaction $U' = U/\kappa$. Three cases were considered, differing by the inclusion of the Hubbard term and the choice of the Ohno parameter r_0 . First, we examined the effect of r_0 to ensure a physically meaningful screening behavior and to evaluate the reliability of the Ohno model in extended π -conjugated systems in conjunction with the pCCD excited states via the EOM-pCCD+S formalism. [92] The value of r_0 controls the range of the electron–electron interaction; a larger r_0 corresponds to stronger screening, while a smaller r_0 emphasizes short-range repulsion. Accurately capturing this screening behavior is essential for correctly predicting excitation energies. Notably, EOM-pCCD+S consistently converged and provided reliable results when the on-site Hubbard term was excluded from the Hamiltonian. The outcomes for a representative set of parameters under this condition are presented in Figures 4a and 4b, where the ground-state pCCD and excited state EOM-pCCD+S methods remain effective over a wide range of U' parameters. The contour plots help identify suitable hopping and interaction parameters that yield excitation energies close to experimental values. In Figure 4a, the on-site Hubbard interaction is excluded and a long-range

Ohno form ($r_0 \approx 1.28$ a.u.) is used. This setup leads to significantly overestimated excitation energies, especially for larger systems. Figure 4b applies a shorter-range Coulomb interaction ($r_0 = 0.25$ a.u.), but still omits the Hubbard U -term. While this correction lowers excitation energies, the model still fails to fully capture electron localization, particularly in larger structures. By comparing panels (a) and (b) in Figure 4, we find that the overall trends in excitation energies remain unchanged; only the converged values of U' shift with changes in the r_0 parameter. This indicates that while the qualitative behavior of the system is governed primarily by the interplay between kinetic and Coulomb terms, the choice of r_0 , which controls the range and strength of the inter-site electron-electron repulsion, affects the absolute energy scales needed to reproduce experimental excitation energies.

After identifying a suitable r_0 , we examined the influence of the on-site Hubbard interaction by including the Hubbard U -term. This step is crucial for ensuring that the ratio U/t remains greater than 1, which places the system in a correlated electron regime. This condition is physically justified for carbon based systems, where electron–electron repulsion plays a dominant role compared to kinetic delocalization. When $U/t < 1$, electron correlation effects are significantly underestimated, and the system behaves more like a free-electron gas or metal, which is inconsistent with the localized character of π -electrons in these molecules. Figure 4c, includes both the Hubbard U -term and the short-range Ohno interaction ($r_0 = 0.25$), resulting in excitation energies that closely match experimental values across all molecules. This demonstrates that both local and nonlocal electron–electron interactions are essential for accurate modeling of excited states in π -conjugated systems.

2. Parameter Fine-Tuning for the Localized Case

While all pCCD-based calculations performed with canonical HF orbitals provide valuable insights, they exhibit certain limitations when applied to the PPP model, particularly in capturing electron correlation effects in system with small HOMO-LUMO gaps accurately. To address these shortcomings, we further investigated the orbital-optimized pCCD (oo-pCCD) approach, which allows for variational optimization of the molecular orbitals alongside the pCCD amplitudes. Additionally, excited-state properties are explored using the linear-response variant of pCCD+S (LR-pCCD+S), providing a reliable and consistent framework for treating correlated excited states across the PAH series.

Figure 3 visualizes the excitation energies as a function of the inter-site interaction parameter

U' , computed using pCCD-optimized orbitals within the PPP model Hamiltonian. The selected structures correspond to those used in HF-based PPP calculations. Note that we kept the hopping and Hubbard terms fixed, with $t = -2.7$ eV, $U = 8$ eV, and $r_0 = 0.25$. The experimental and semi-experimental excitation energies are shown with red and blue stars, respectively, with their values annotated for clarity. The results show a consistent trend for all structures, and pCCD excitation energies decrease with increasing U' . This behavior reflects the influence of electron–electron repulsion on electronic structures. The agreement between pCCD results and experimental data is generally good, and for all structures except $C_{36}H_{18}$, the ratio of U'/t is larger than one, indicating that these systems are in a strongly-correlated regime where interaction effects dominate over electron delocalization. Compared with the experimental excitation energies (see Table I), the optimal choice for the U' shift in the localized pCCD-optimized basis is $U' = 2.9$. If not mentioned otherwise, we will employ the aforementioned values ($t = -2.7$ eV, $U = 8$ eV, $U' = 2.9$, and $r_0 = 0.25$) in orbital-optimized pCCD-based calculations.

B. CI Calculations with Canonical HF Orbitals

To evaluate the performance of different configuration interaction (CI) methods on PAH systems, we performed CIS, CID, and CISD calculations using a common set of PPP parameters derived from experimental excitation energies. Specifically, we used a hopping integral $t = -4.1$ eV, an on-site repulsion parameter $U = 6.0$ eV, and a dielectric screening factor $\kappa = 2$. All calculations used the canonical HF orbitals.

TABLE I: CI excitation energies (CID/PPP, CID/PPP and CISD/PPP) in (eV) for PAHs from Figure 1 using canonical HF orbitals with fixed PPP parameters ($t = -4.1$ eV, $U = 6.0$ eV, $\kappa = 2$). Experimental values are included where available.

Structure	CIS	CID	CISD	Exp. [83, 102, 103]
$C_{22}H_{12}$	2.29	2.86	2.61	–
$C_{28}H_{14}$	2.98	2.56	3.35	3.38
$C_{30}H_{14}$	2.47	1.31	2.86	3.02
$C_{32}H_{16}$	2.05	0.22	2.51	–
$C_{36}H_{18}$	1.11	0.73	0.58	–

Table I shows the excitation energies obtained by different CI methods. CIS only includes single excitations from the reference state and thus lacks a proper description of electron correlation,

especially the dynamic correlation associated with (broken) electron pairs. In contrast, CID, which includes only double excitations, often overestimates correlation, particularly in larger systems, as seen in the unphysically low excitation energies for $\text{C}_{32}\text{H}_{16}$ and $\text{C}_{36}\text{H}_{18}$. CISD, which incorporates both single and double excitations, shows the best overall agreement with experimental data when available. In the case of $\text{C}_{28}\text{H}_{14}$ and $\text{C}_{30}\text{H}_{14}$, CISD excitation energies (3.35 eV and 2.86 eV, respectively) closely match the corresponding experimental values (3.38 eV and 3.02 eV), which validates the PPP model Hamiltonian in describing π -conjugated systems.

C. CI and EOM-pCCD+S Results with pCCD Orbitals

To evaluate the reliability of pCCD-based methods, we performed post-pCCD calculations using optimized pCCD orbitals. Configuration interaction methods (CID and CISD) were applied on top of the pCCD-optimized reference determinant, as well as the EOM-pCCD+S approach for excited states. These calculations employed the same fixed PPP parameters used earlier ($t = -4.1$ eV, $U = 6.0$ eV, $\kappa = 2$). The computed excitation energies are listed in Table II, together with available experimental data.

TABLE II: Excitation energies (in eV) obtained from the CID/PPP, CISD/PPP, and EOM-pCCD+S/PPP methods using the pCCD-optimized orbitals and molecules from Figure 1.

Parameters: $t = -4.1$ eV, $U = 6.0$ eV, $\kappa = 2$.

Structure	CID	CISD	EOM-pCCD+S	Exp. [83, 102, 103]
$\text{C}_{22}\text{H}_{12}$	2.96	2.55	2.76	—
$\text{C}_{28}\text{H}_{14}$	2.56	3.30	3.40	3.38
$\text{C}_{30}\text{H}_{14}$	1.56	2.81	2.88	3.02
$\text{C}_{32}\text{H}_{16}$	1.56	2.81	2.88	—
$\text{C}_{36}\text{H}_{18}$	0.10	1.14	1.44	—

- For all structures examined, the inclusion of single excitations in CISD significantly lowers the excitation energies compared to CID, highlighting the importance of single excitations in the description of excited states using CI-type methods.

The EOM-pCCD+S results fall between the CID and CISD values, suggesting that EOM-pCCD+S effectively models the electronic structures of the ground and excited states on an equal footing while maintaining computational efficiency. Furthermore, it yields excitation energies in good agreement

with experimental results. In particular, for the $C_{28}H_{14}$ and $C_{30}H_{14}$ systems, the EOM-pCCD+S excitation energies differ by only 0.02–0.14 eV from experimental values. This level of agreement is notable given the simplified nature of the PPP Hamiltonian and the approximate character of the EOM-pCCD+S method. However, discrepancies (between CISD and EOM-pCCD+S) increase for larger systems like $C_{36}H_{18}$, indicating a potential need for higher-order excitations or improved parametrizations for larger π -conjugate systems.

To further benchmark the accuracy of the EOM-pCCD+S method paired with the PPP Hamiltonian, we compared our EOM-pCCD+S excitation energies (with the pCCD-optimized orbitals) with the MCSCF results from Ref. 83. Table III highlights the impact of the Ohno parameter r_0 on the performance of EOM-pCCD+S relative to both high-level MCSCF results and experimental excitation energies. The excitation energies computed using EOM-pCCD+S agree well with the MCSCF values, especially when the Ohno parameter $r_0 = 0.25$ is used. Overall, the EOM-pCCD+S excitation energies closely track the MCSCF values, especially for intermediate-sized systems. Reducing r_0 to 0.25, ensuring a proper overlap value for C–C bonding [82], often results in excitation energies that are slightly lower and, in some cases (e.g., $C_{30}H_{14}$), closer to the experimental reference. This sensitivity to the parameterization reflects the delicate balance between short- and long-range Coulomb interactions in π -conjugated systems. For the largest system studied, $C_{36}H_{18}$, both parameterizations result in EOM-pCCD+S to underestimate the excitation energy by about 0.4 eV compared to the MCSCF reference. This discrepancy can originate from the EOM-pCCD+S method or the parameterization of the PPP Hamiltonian that inappropriately describe electron correlation effects, or the choice of the active space in the MCSCF optimization procedure. Nonetheless, our data demonstrates that the EOM-pCCD+S method, combined with carefully chosen PPP parameters and orbital optimization, can serve as a computationally affordable alternative to multi-reference approaches for modeling low-lying excited states in π -extended systems.

D. Electronic Spectra of PAHs using Canonical HF Orbitals

To investigate the electronic spectra of selected PAHs shown in Figure 1, we computed oscillator strengths using the linear-response ansatz within the LR-pCCD+S framework for two systems, $C_{32}H_{16}$ and $C_{36}H_{18}$, and compared the resulting theoretical spectra with available experimental intensity data. [104, 105]

Since the PPP model Hamiltonian does not involve an explicit basis set, the first step in obtaining

TABLE III: Comparison of excitation energies (in eV) obtained from MCSCF [83] and EOM-pCCD+S using two different Ohno parameterizations (molecules from Figure 1). Experimental values are also reported. The parameters used in EOM-pCCD+S are: $t = -2.7$ eV, $U = 8$ eV, and $U' = 0.8$ for $r_0 = 1.28$, and $U' = 2.9$ for $r_0 = 0.25$.

Structure	MCSCF	EOM-pCCD+S ^a		Exp. [83]
		$r_0 = 1.28$	$r_0 = 0.25$	
C ₂₂ H ₁₂	3.39	3.35	3.23	–
C ₂₈ H ₁₄	3.42	3.32	3.26	3.38
C ₃₀ H ₁₄	2.95	2.86	2.94	3.02
C ₃₂ H ₁₆	2.93	2.85	2.90	–
C ₃₆ H ₁₈	2.70	2.30	2.30	–

a) Excitation energies computed using EOM-pCCD+S based on an orbital-optimized pCCD (oo-pCCD) reference.

oscillator strengths is to compute site-dependent momentum integrals (the theoretical details of this approach are outlined in Section II). To validate the accuracy of our implementation, we calculated ground-state dipole moments for several small molecules both with and without basis sets and compared the results against data from Ref. [96].

TABLE IV: Ground-state dipole moments (in Debye) for selected molecules, computed using Hartree–Fock (HF) and pCCD orbitals with and without molecular basis set. The physical model Hamiltonians use a hopping parameter of $t = -2.7$ eV and the listed U values.

Molecule (U)	PPP		STO-3G		cc-pVDZ	
	HF	pCCD	HF	pCCD	HF	pCCD
Benzene (8.0 eV)	0.000	0.000	0.000	0.000	0.000	0.000
Furan (8.0 eV)	0.717	1.360	0.426	0.609	0.748	0.275
CO (7.2 eV)	0.300	0.296	0.264	0.526	0.470	0.125

Table IV presents the ground-state dipole moments of three small molecules—benzene, furan, and carbon monoxide (CO)—computed using Hartree-Fock (HF) and pCCD orbitals across various methods, with and without atom-centered basis sets. Benzene, with its high symmetry (D_{6h}) and zero dipole moment, serves as an internal consistency check due to its lack of permanent polarization. For small polar molecules like furan and CO, the calculated dipole moments exhibit significant variation depending on the method and basis set employed.

Furan, a five-membered heterocyclic aromatic compound with a planar ring comprising four carbon atoms and one oxygen, is a prototypical π -electron system, making it well-suited for the PPP model within our pCCD/PPP framework. In contrast, CO poses a significant challenge for the PPP model, as its electronic structure and dipole moment require large molecular basis sets and high-order coupled cluster methods (e.g., CCSDT) to achieve reliable descriptions. [9, 98]

For furan, the PPP model with HF orbitals predicts a dipole moment of 0.717 D, while performing a ground-state pCCD calculation increases it to 1.360 D. In contrast, using atom-centered basis sets like STO-3G and cc-pVDZ, HF yields smaller dipole moments of 0.428 D and 0.748 D, respectively, while pCCD reduces these values to 0.609 D (STO-3G) and 0.275 D (cc-pVDZ).

For carbon monoxide (CO), the PPP model combined with HF and pCCD calculations yields nearly identical dipole moments of 0.300 D and 0.296 D, respectively. However, ab initio calculations reveal significant discrepancies, underscoring the sensitivity of CO’s dipole moment to both electron correlation and basis set choice.

These findings highlight the interplay between correlation, basis set quality, and model choice in dipole moment predictions. With this accuracy established, we proceed to investigate oscillator strengths using the linear response coupled cluster (LR-CC) approach, which is essential for characterizing the intensity and spectral features of electronic excitations in π -electron systems like furan and related polycyclic aromatic hydrocarbons (PAHs). To that end, we employed the LR-pCCD+S approach to compute oscillator strengths and analyzed the UV-Vis absorption spectra of polycyclic aromatic hydrocarbons (PAHs). Oscillator strengths are critical for interpreting absorption features in molecular spectra, and the LR-pCCD+S method, integrated with the PPP model Hamiltonian, provides a computationally efficient approach for modeling these properties in π -electron systems.

Figure 5 presents experimental and theoretical UV-Vis absorption spectra for $C_{28}H_{14}$ and $C_{30}H_{14}$. The corresponding numerical data is in the Supplemental Material [106]. Panels (a) and (c) display experimental spectra, while panels (b) and (d) show the corresponding theoretical spectra computed using LR-pCCD+S with the PPP model. Overall, the computational results reproduce the qualitative features of the experimental spectra, particularly in terms of peak positions. For $C_{28}H_{14}$, Figure 5(a) exhibits a strong absorption band at approximately 315 nm, which the theoretical spectrum in Figure 5(b) captures reasonably well, predicting major peaks at 275, 320, and 365 nm. The agreement in peak positions is good, though the PPP-based model overestimates the oscillator strength of the short-wavelength transition (275 nm), likely due to the neglect of dynamic electron correlation.

For $C_{30}H_{14}$, Figure 5(c) shows multiple absorption bands between 320–340 nm and a broader

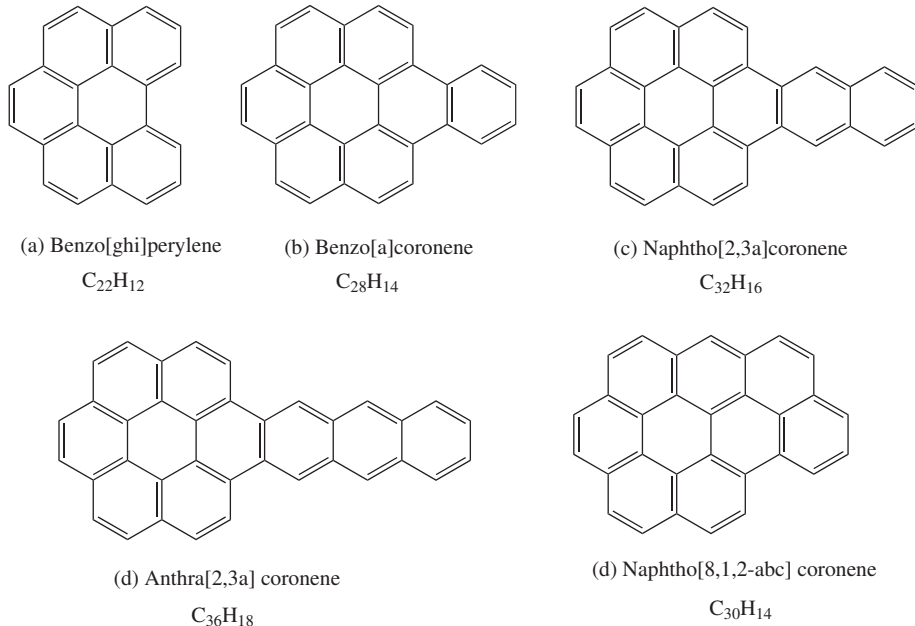


FIG. 1: Representative structures of polycyclic aromatic hydrocarbons (PAHs) considered in this study. The hydrogen atoms are not explicitly shown.

band from 380–400 nm. The theoretical spectrum in Figure 5(d) reflects these trends, predicting a dominant transition at 285 nm and weaker transitions at approximately 320 and 400 nm. Discrepancies in peak intensities and shapes between experimental and theoretical spectra are expected when using simplified models like the PPP Hamiltonian with LR-pCCD+S, as these approaches do not fully account for dynamic correlation and higher-order electronic interactions. Despite these limitations, the LR-pCCD+S method within the PPP framework effectively captures the overall spectral features and primary electronic excitations, demonstrating its utility for predicting the optical properties of large PAHs. To conclude, our approach provides a robust and efficient platform for studying the electronic structure and spectroscopic properties of complex organic molecules, with applications in designing novel optoelectronic materials.

E. Conclusion and Outlook

In this work, we present the first integration of pCCD-based methods, implemented in the PyBEST software package, with the PPP model Hamiltonian. This novel combination leverages the strengths of pCCD’s variational orbital optimization protocol to enable cost-effective and reliable modeling of π -extended systems with small HOMO-LUMO gaps, offering advantages over

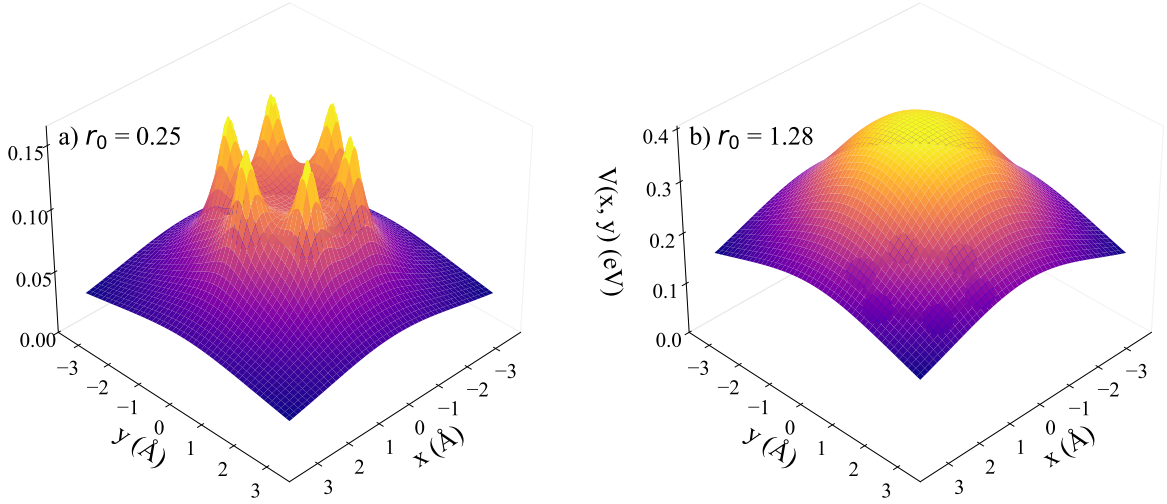


FIG. 2: Three-dimensional Ohno potential fields for the carbon atoms in benzene (C_6H_6), projected onto the molecular plane for two different screening lengths r_0 ; (a) $r_0 = 0.25 \text{ \AA}$, and (b) $r_0 = 1.28 \text{ \AA}$. The potential is calculated by summing pairwise Ohno interactions over all non-hydrogen atoms. Carbon atoms are shown with spheres. As r_0 increases, the potential becomes more spatially diffuse, highlighting the impact of screening on the effective interaction range.

conventional electronic structure methods. [9, 10, 77]

The pCCD approach optimizes all orbitals variationally, resulting in a well-balanced basis across different molecular sizes. This contrasts with methods like Multi-Reference Configuration Interaction with Singles and Doubles (MRCISD), which require a carefully defined active space and are less adaptable to large or diverse systems. Due to the localized nature of the pCCD-optimized basis, the standard PPP model parametrization, typically defined for canonical HF orbitals, must be reoptimized to ensure accuracy.

To achieve this, we optimized the PPP model parameters (U , t , and κ) using experimental excitation energies of selected polycyclic aromatic hydrocarbons (PAHs), specifically Benzo[a]coronene and Naphtho[8,1,2-abc]coronene, as reference data. Our predicted electronic spectra, encompassing excitation energies and oscillator strengths, accurately reproduce the qualitative features of the experimental UV-Vis spectra for Benzo[a]coronene and Naphtho[8,1,2-abc]coronene. Additionally, we provide new theoretical spectra for Benzo[ghi]perylene, Naphtho[2,3-a]coronene, and Anthra[2,3-a]coronene, offering insights into their electronic properties.

Our numerical results demonstrate that the pCCD/PPP-based computational framework is a

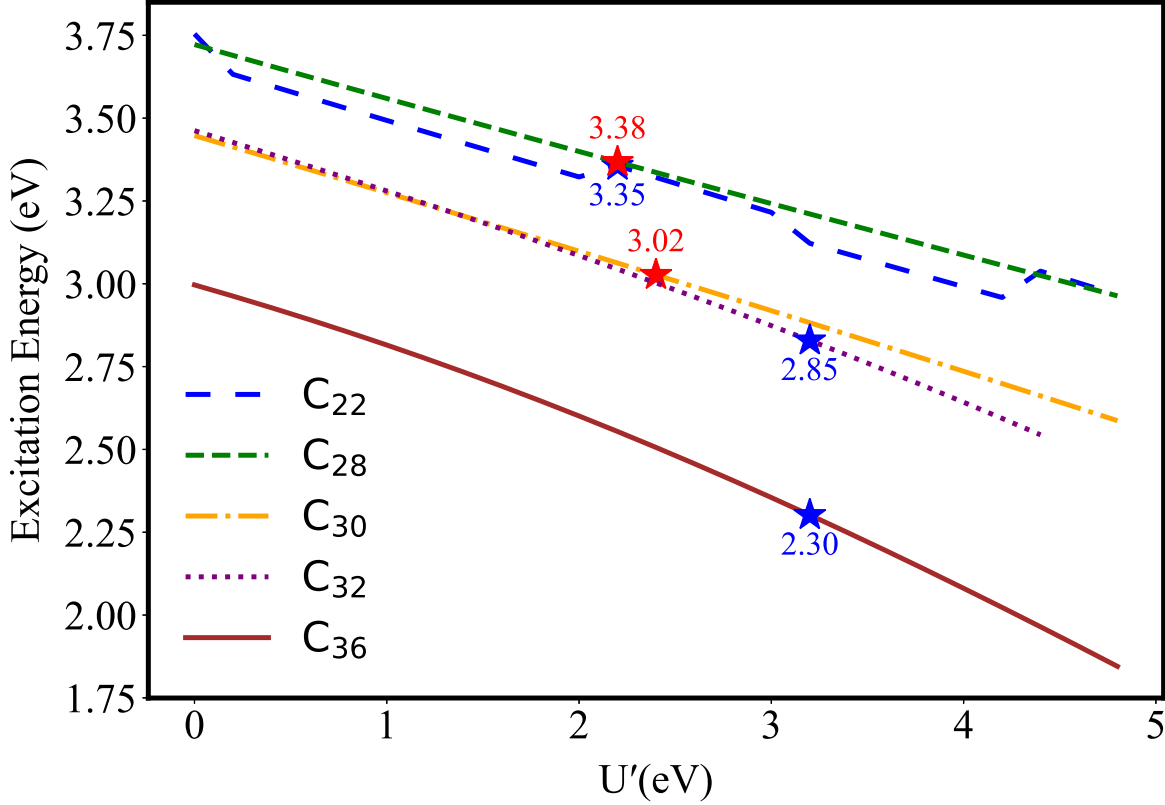


FIG. 3: Dependence of the excitation energy on the global scaling factor $U' = \frac{U}{\kappa}$ used in the PPP Hamiltonian for EOM-pCCD+S using the pCCD optimized orbitals. Experimental excitation energies are indicated with a star.

powerful tool for predicting the electronic structure and spectroscopic properties of complex organic molecules. This approach provides a robust and predictive platform for designing novel organic electronic materials, such as those used in organic solar cells and light-emitting diodes, advancing the development of next-generation optoelectronic technologies.

ACKNOWLEDGMENTS

Z. K., S. A., and P. T. acknowledge financial support from the SONATA BIS research grant from the National Science Centre, Poland (Grant No. 2021/42/E/ST4/00302). Funded/Co-funded by the European Union (ERC, DRESSED-pCCD, 101077420). Views and opinions expressed are, however, those of the author(s) only and do not necessarily reflect those of the European Union or the European Research Council. Neither the European Union nor the granting authority can be

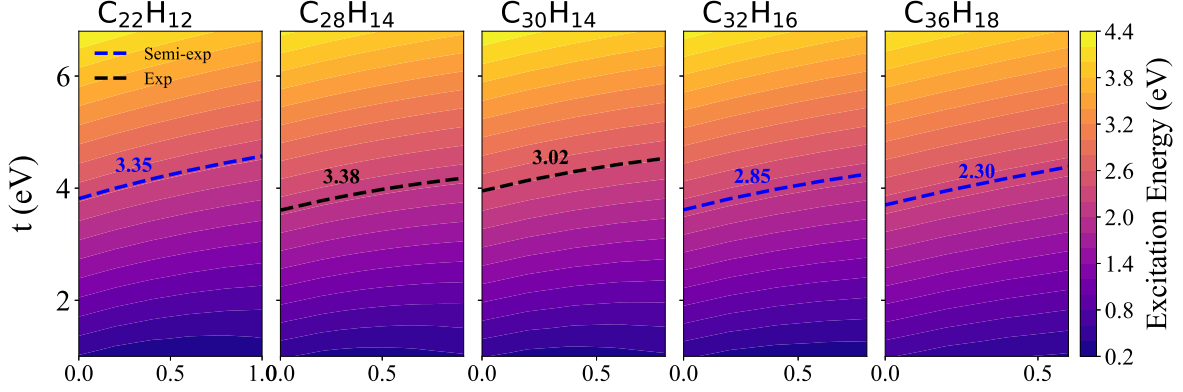
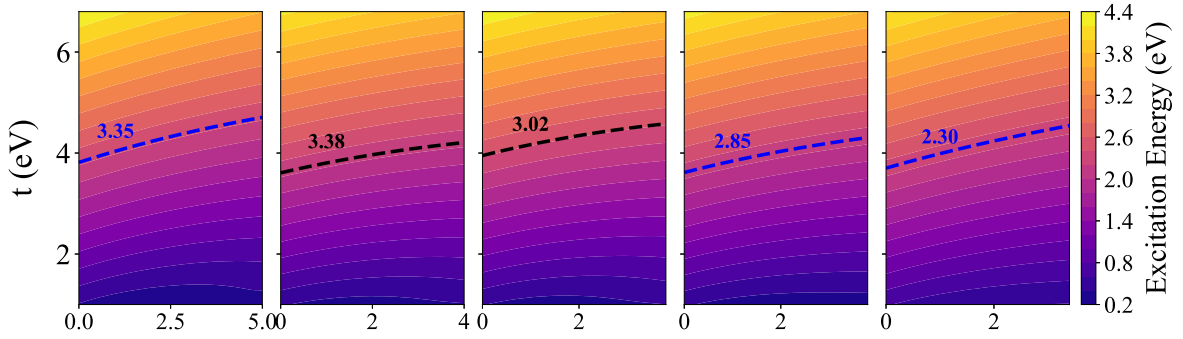
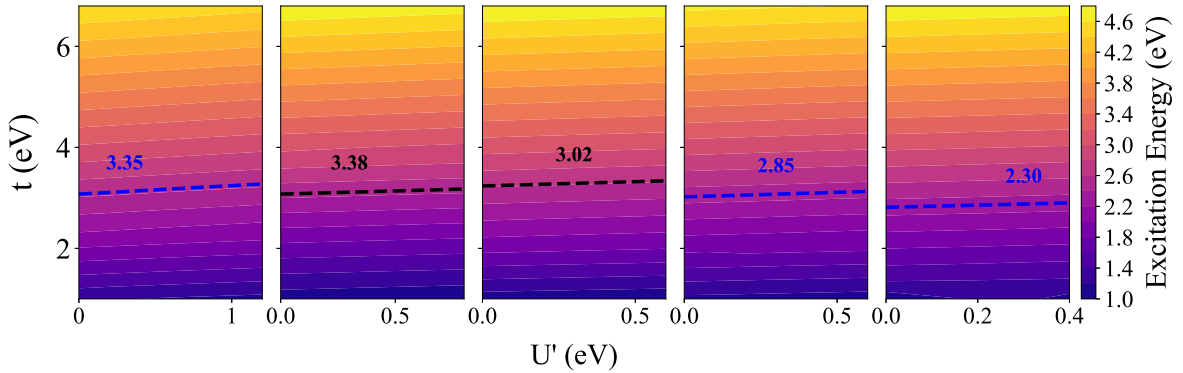
(a) Without the Hubbard term and $r_0 \approx 1.28$ a.u.(b) Without the Hubbard term and $r_0 = 0.25$ a.u.(c) With the Hubbard term and $r_0 = 0.25$ a.u.

FIG. 4: Contour plots of the first excitation energies computed using EOM-pCCD+S with canonical Hartree–Fock orbitals, shown as a function of the transfer integral t and the Ohno-scaled inter-site Coulomb term U' . Three parameter regimes are compared, (a) without the Hubbard term and $r_0 \approx 1.28$ a.u., (b) without the Hubbard term and an Ohno parameter of $r_0 = 0.25$ a.u., and (c) with the Hubbard term ($U = 8$ eV) and $r_0 = 0.25$ a.u. The black dashed lines indicate the experimental excitation energies for $C_{28}H_{14}$ and $C_{30}H_{14}$. For the other structures with blue dashed lines, the corresponding excitation energies were determined by aligning them with similar features in the experimental spectra (labeled as semi-exp), following the approach used in Ref. [103].

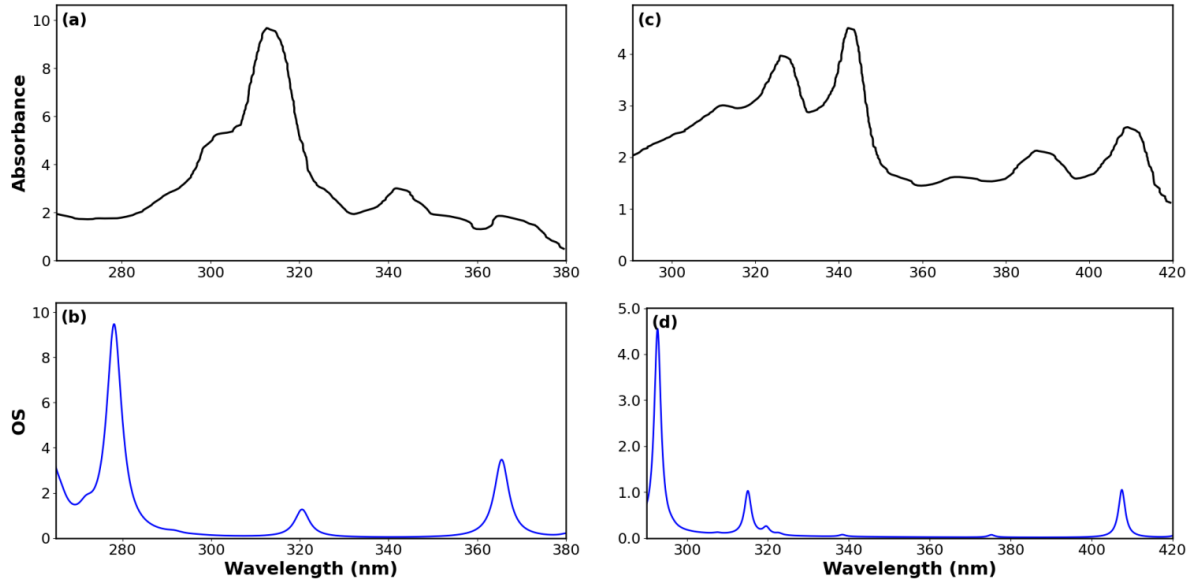


FIG. 5: Experimental UV spectra of (a) Benzo[a]coronene and (c) Naphtho[8,1,2-abc]coronene, compared with OOpCCD results in (b) and (d), respectively.

held responsible for them.

-
- [1] T. Körzdörfer and J.-L. Brédas, *Acc. Chem. Res.* **47**, 3284 (2014).
 - [2] Y. Cui, P. Zhu, X. Liao, and Y. Chen, *J. Mater. Chem. C* **8**, 15920 (2020).
 - [3] V. Bhat, C. P. Callaway, and C. Risko, *Chem. Rev.* **123**, 7498 (2023).
 - [4] R. J. Bartlett and J. F. Stanton, *Rev. Comput. Chem.* **5**, 165 (1994).
 - [5] K. Boguslawski, P. Tecmer, O. Legeza, and M. Reiher, *J. Phys. Chem. Lett.* **3**, 3129 (2012).
 - [6] G. Fano, F. Ortolani, and L. Ziosi, *J. Chem. Phys.* **108**, 9246 (1998).
 - [7] J. Hachmann, J. J. Dorando, M. Avilés, and G. K.-L. Chan, *J. Chem. Phys.* **127**, 134309 (2007).
 - [8] M. Timár, G. Barcza, F. Gebhard, L. Veis, and Ö. Legeza, *Phys. Chem. Chem. Phys.* **18**, 18835 (2016).
 - [9] S. Jahani, K. Boguslawski, and P. Tecmer, *RSC Adv.* **13**, 27898 (2023).
 - [10] P. Tecmer, M. Gałyńska, L. Szczuczko, and K. Boguslawski, *J. Phys. Chem. Lett.* **14**, 9909 (2023).
 - [11] Helgaker, T. and Jørgensen, P. and Olsen, J., *Molecular electronic-structure theory* (Wiley, New York, 2000).
 - [12] Z. Li and F. A. Evangelista, *Annu. Rev. Phys. Chem.* **68**, 361 (2017).
 - [13] M. Motta and S. Zhang, *WIREs Comput. Mol. Sci.* **8**, e1364 (2018).
 - [14] B. Roos, P. Taylor, and P. Siegbahn, *Chem. Phys.* **48**, 157 (1980).
 - [15] P. J. Knowles and H.-J. Werner, *Chem. Phys. Lett.* **115**, 259 (1985).

- [16] P. G. Szalay, T. Müller, G. Gidofalvi, H. Lischka, and R. Shepard, *Chem. Rev.* **112**, 108 (2012).
- [17] S. R. White, *Phys. Rev. Lett.* **69**, 2863 (1992).
- [18] S. R. White, *Phys. Rev. B* **48**, 10345 (1993).
- [19] S. R. White and R. L. Martin, *J. Chem. Phys.* **110**, 4127 (1999).
- [20] K. H. Marti and M. Reiher, *Z. Phys. Chem.* **224**, 583 (2010).
- [21] G. Barcza, O. Legeza, K. H. Marti, and M. Reiher, *Phys. Rev. A* **83**, 012508 (2011).
- [22] O. Legeza, R. M. Noack, J. Sólyom, and L. Tincani, in *Computational Many-Particle Physics*, Lect. Notes Phys., Vol. 739, edited by H. Fehske, R. Schneider, and A. Weiße (Springer, Berlin/Heidelberg, 2008) pp. 653–664.
- [23] S. Szalay, M. Pfeffer, V. Murg, G. Barcza, F. Verstraete, R. Schneider, and Ö. Legeza, *Int. J. Quantum Chem.* **115**, 1342 (2015).
- [24] G. K.-L. Chan and S. Sharma, *Annu. Rev. Phys. Chem.* **62**, 465 (2011).
- [25] S. Wouters and D. Van Neck, *Eur. Phys. J. D* **68**, 272 (2014).
- [26] Ö. Legeza, R. Noack, J. Sólyomand, L. Tincani, *Computational Many-Particle Physics*, Vol. 739 (Springer, Berlin/Heidelberg, 2005) pp. 653–664.
- [27] W. Hu and G. K.-L. Chan, *J. Chem. Theory Comput.* **11**, 3000 (2015).
- [28] R. G. Parr and W. Yang, Oxford University Press (1989).
- [29] J. Čížek, *J. Chem. Phys.* **45**, 4256 (1966).
- [30] J. Čížek, *Adv. Chem. Phys.* **14**, 35 (1969).
- [31] J. Čížek and J. Paldus, *Int. J. Quantum Chem.* **5**, 359 (1971).
- [32] J. Paldus, J. Cizek, and I. Shavitt, *Phys. Rev. A* **5**, 50 (1972).
- [33] R. J. Bartlett and M. Musiał, *Rev. Mod. Phys.* **79**, 291 (2007).
- [34] Z. L. Cai, K. Sendt, and J. R. Reimers, *J. Chem. Phys.* **117**, 5543 (2002).
- [35] S. Tortorella, M. M. Talamo, A. Cardone, M. Pastore, and F. De Angelis, *J. Phys.: Condens. Matter* **28**, 074005 (2016).
- [36] E. Hückel, *Z. Phys.* **70**, 204 (1931).
- [37] E. Hückel, *Z. Phys.* **76**, 628 (1932).
- [38] J. Hubbard, *Proc. R. Soc. Lond. A* **276**, 238 (1963).
- [39] R. Pariser and R. G. Parr, *J. Chem. Phys.* **21**, 466 (1953).
- [40] R. Pariser and R. G. Parr, *J. Chem. Phys.* **21**, 767 (1953).
- [41] J. A. Pople, *Trans. Faraday Soc.* **49**, 1375 (1953).
- [42] K. Jug, *Int. J. Quantum Chem.* **37**, 403 (1990).
- [43] R. J. Bursill, C. Castleton, and W. Barford, *Chem. Phys. Lett.* **294**, 305 (1998).
- [44] R. Podeszwa, L. Z. Stolarczyk, K. Jankowski, and K. Rubiniec, *Theor. Chem. Acc.* **109**, 309 (2003).
- [45] P. Sony and A. Shukla, *Phys. Rev. B* **75**, 155208 (2007).
- [46] G. Chiappe, E. Louis, and E. San-Fabián, *J. Phys.: Condens. Matter* **27**, 465301 (2015).
- [47] K. Jorner, R. Pollice, C. Lavigne, and A. Aspuru-Guzik, *J. Phys. Chem. A* **128**, 2445 (2024).

- [48] A. B. Zakharov, V. V. Ivanov, and L. Adamowicz, *J. Phys. Chem. C* **118**, 8111 (2014).
- [49] P. R. Surján, *Correlation and localization*, 63 (1999).
- [50] P. R. Surján, Á. Szabados, P. Jeszenszki, and T. Zoboki, *J. Math. Chem.* **50**, 534 (2012).
- [51] E. Xu and S. Li, *J. Chem. Phys.* **139**, 174111 (2013).
- [52] D. W. Small, K. V. Lawler, and M. Head-Gordon, *J. Chem. Theory Comput.* **10**, 2027 (2014).
- [53] P. Tecmer and K. Boguslawski, *Phys. Chem. Chem. Phys.* **24**, 23026 (2022).
- [54] P. A. Johnson, P. A. Limacher, T. D. Kim, M. Richer, R. A. Miranda-Quintana, F. Heidar-Zadeh, P. W. Ayers, P. Bultinck, S. De Baerdemacker, and D. Van Neck, *Comput. Theor. Chem.* **1116**, 207 (2017).
- [55] S. Lehtola and M. Head-Gordon, *Mol. Phys.*, e2489096 (2025).
- [56] P. A. Limacher, P. W. Ayers, P. A. Johnson, S. De Baerdemacker, D. Van Neck, and P. Bultinck, *J. Chem. Theory Comput.* **9**, 1394 (2013).
- [57] T. Stein, T. M. Henderson, and G. E. Scuseria, *J. Chem. Phys.* **140** (2014).
- [58] K. Boguslawski, P. Tecmer, P. W. Ayers, P. Bultinck, S. De Baerdemacker, and D. Van Neck, *Phys. Rev. B* **89**, 201106(R) (2014).
- [59] K. Boguslawski, P. Tecmer, P. A. Limacher, P. A. Johnson, P. W. Ayers, P. Bultinck, S. De Baerdemacker, and D. Van Neck, *J. Chem. Phys.* **140**, 214114 (2014).
- [60] P. A. Limacher, T. D. Kim, P. W. Ayers, P. A. Johnson, S. De Baerdemacker, D. Van Neck, and P. Bultinck, *Mol. Phys.* **112**, 853 (2014).
- [61] K. Boguslawski, P. Tecmer, P. W. Ayers, P. Bultinck, S. De Baerdemacker, and D. Van Neck, *J. Chem. Theory Comput.* **10**, 4873 (2014).
- [62] T. M. Henderson, I. W. Bulik, T. Stein, and G. E. Scuseria, *J. Chem. Phys.* **141**, 244104 (2014).
- [63] P. Limacher, P. Ayers, P. Johnson, S. De Baerdemacker, D. Van Neck, and P. Bultinck, *Phys. Chem. Chem. Phys.* **16**, 5061 (2014).
- [64] A. J. Garza, I. W. Bulik, T. M. Henderson, and G. E. Scuseria, *Phys. Chem. Chem. Phys.* **17**, 22412 (2015).
- [65] K. Boguslawski and P. W. Ayers, *J. Chem. Theory Comput.* **11**, 5252 (2015).
- [66] A. Leszczyk, M. Máté, Ö. Legeza, and K. Boguslawski, *J. Chem. Theory Comput.* **18**, 96 (2022).
- [67] P. Tecmer, K. Boguslawski, P. A. Limacher, P. A. Johnson, M. Chan, T. Verstraelen, and P. W. Ayers, *J. Phys. Chem. A* **118**, 9058 (2014).
- [68] P. Tecmer, K. Boguslawski, and P. W. Ayers, *Phys. Chem. Chem. Phys.* **17**, 14427 (2015).
- [69] A. Nowak, i. Legeza, and K. Boguslawski, *J. Chem. Phys.* **154**, 084111 (2021).
- [70] K. Boguslawski and P. Tecmer, *J. Chem. Theory Comput.* **13**, 5966 (2017).
- [71] P. Tecmer, K. Boguslawski, M. Borkowski, P. S. Żuchowski, and D. Kędziera, *Int. J. Quantum Chem.* **119**, e25983 (2019).
- [72] A. Nowak, P. Tecmer, and K. Boguslawski, *Phys. Chem. Chem. Phys.* **21**, 19039 (2019).
- [73] A. Leszczyk, T. Dome, P. Tecmer, D. Kędziera, and K. Boguslawski, *Phys. Chem. Chem. Phys.* **24**,

- 21296 (2022).
- [74] A. Nowak and K. Boguslawski, *Phys. Chem. Chem. Phys.* **25**, 7289 (2023).
 - [75] R. Chakraborty, K. Boguslawski, and P. Tecmer, *Phys. Chem. Chem. Phys.* **25**, 25377 (2023).
 - [76] M. Gałyńska, M. M. F. de Moraes, P. Tecmer, and K. Boguslawski, *Phys. Chem. Chem. Phys.* **26**, 18918 (2024).
 - [77] M. Gałyńska, P. Tecmer, and K. Boguslawski, *J. Phys. Chem. A* **128**, 11068 (2024).
 - [78] R. D. Pandey, M. M. F. de Moraes, K. Boguslawski, and P. Tecmer, *J. Chem. Theory Comput.* **21**, 5049 (2025).
 - [79] L. Szczuczko, M. Gałyńska, M. H. Kriebel, P. Tecmer, and K. Boguslawski, *J. Chem. Theory Comput.* **21**, 4506 (2025).
 - [80] P. Sony and A. Shukla, *Comput. Phys. Commun.* **181**, 821 (2010).
 - [81] V. Chuiko, A. D. S. Richards, G. Sánchez-Díaz, M. Martínez-González, W. Sanchez, G. B. Da Rosa, M. Richer, Y. Zhao, W. Adams, P. A. Johnson, F. Heidar-Zadeh, and P. W. Ayers, *J. Chem. Phys.* **161**, 132503 (2024).
 - [82] K. Ohno, *Theor. Chim. Acta* **2**, 219 (1964).
 - [83] P. Bhattacharyya, D. K. Rai, and A. Shukla, *J. Phys. Chem. C* **124**, 14297 (2020).
 - [84] H. Chakraborty and A. Shukla, *J. Phys. Chem. A* **117**, 14220 (2013).
 - [85] S. Lambie, D. Kats, D. Usvyat, and A. Alavi, *J. Chem. Phys.* **162**, 114112 (2025).
 - [86] K. Boguslawski, P. Tecmer, G. Barcza, O. Legeza, and M. Reiher, *J. Chem. Theory Comput.* **9**, 2959 (2013).
 - [87] V. V. Ivanov, D. I. Lyakh, and L. Adamowicz, *Phys. Chem. Chem. Phys.* **11**, 2355 (2009).
 - [88] B. Jeziorski, *Mol. Phys.* **108**, 3043 (2010).
 - [89] D. I. Lyakh, M. Musiał, V. F. Lotrich, and J. Bartlett, *Chem. Rev.* **112**, 182 (2012).
 - [90] A. Köhn, M. Hanauer, L. A. Mück, T.-C. Jagau, and J. Gauss, *WIREs Comp. Mol. Sci.* **3**, 176 (2013).
 - [91] K. Boguslawski, P. Tecmer, and Ö. Legeza, *Phys. Rev. B* **94**, 155126 (2016).
 - [92] K. Boguslawski, *J. Chem. Phys.* **145**, 234105 (2016).
 - [93] K. Boguslawski, *J. Chem. Phys.* **147**, 139901 (2017).
 - [94] S. Ahmadkhani, K. Boguslawski, and P. Tecmer, *J. Chem. Theory Comput.* **20**, 10443 (2024).
 - [95] K. Boguslawski, *J. Chem. Theory Comput.* **15**, 18 (2019).
 - [96] R. Chakraborty, M. M. F. de Moraes, K. Boguslawski, A. Nowak, J. Świerczyński, and P. Tecmer, *J. Chem. Theory Comput.* **20**, 4689 (2024).
 - [97] R. Daudel, R. Lefebvre, C. Moser, and S. A. Rice, *Phys. Today* **13**, 56 (1960).
 - [98] R. Chakraborty, S. Ahmadkhani, J. Świerczyński, K. Boguslawski, and P. Tecmer, *J. Phys. Chem. A* **129**, 6713 (2025).
 - [99] K. Boguslawski, A. Leszczyk, A. Nowak, F. Brzęk, P. S. Żuchowski, D. Kędziera, and P. Tecmer, *Comput. Phys. Commun.* **264**, 107933 (2021).
 - [100] K. Boguslawski, F. Brzęk, R. Chakraborty, K. Cieślak, S. Jahani, A. Leszczyk, A. Nowak, E. Sujkowski,

- J. Świerczyński, S. Ahmadkhani, D. Kędziera, M. H. Kriebel, P. S. Żuchowski, and P. Tecmer, *Comput. Phys. Commun.* **297**, 109049 (2024).
- [101] M. Chandross and S. Mazumdar, *Phys. Rev. B* **55**, 1497 (1997).
- [102] J. C. Fetzer, W. R. Biggs, and K. Jinno, *Chromatographia* **21**, 439 (1986).
- [103] S. P. Bagley and M. J. Wornat, *Energy & Fuels* **27**, 1321 (2013).
- [104] W. E. Acree, S. A. Tucker, A. I. Zvaigzne, K. W. Street, J. C. Fetzer, and H.-F. Grutzmacher, *Appl. Spectrosc.* **44**, 477 (1990).
- [105] J. C. Fetzer, *Pol. Aromat. Compd.* **27**, 143 (2007).
- [106] (2025), see Supplemental Material at [URL will be inserted by publisher] for EOM-pCCD+S UV-Vis absorption spectra for $C_{28}H_{14}$ and $C_{30}H_{14}$.